Title

ANALYTICAL STUDY OF A HIGH RESOLUTION POSITRON RING DETECTOR SYSTEM FOR TRANSAXLAL RECONSTRUCTION TOMOGRAPHY

Authors

Derenzo, Stephen E.
Zaklad, Haim
Budinger, Thomas F.

Publication Date

1975-03-01

Submitted to Journal of Nuclear Medicine

LBL-2859
Preprint

ANALYTICAL STUDY OF A HIGH RESOLUTION POSITRON RING DETECTOR SYSTEM FOR TRANSAXIAL RECONSTRUCTION TOMOGRAPHY

DONNER LABORATORY

Stephen E. Derenzo, Haim Zaklad, and Thomas F. Budinger

March 1975

Prepared for the U. S. Atomic Energy Commission
under Contract W-7405-ENG-48

DISCLAIMER

ANALYTICAL STUDY OF A HIGH RESOLUTION POSITRON RING DETECTOR SYSTEM FOR TRANSAXIAL RECONSTRUCTION TOMOGRAPHY

Stephen E. Derenzo, Haim Zaklad, and Thomas F. Budinger

Lawrence Berkeley Laboratory
University of California
Berkeley, California 94720

Running Head: POSITRON RECONSTRUCTION TOMOGRAPHY

For reprints contact:

S.E. Derenzo
50B-5226
University of California
Lawrence Berkeley Laboratory
Berkeley California 94720

ABSTRACT

This paper presents an analytical study of a high resolution positron ring detector system for transaxial reconstruction tomography. Our goal is a combination of good spatial resolution, high sensitivity, rejection of scattered gamma rays, variable section thickness, and the minimization of the number of photomultipliers and coincidence circuits. A circular ring of 280 NaI(Tl) crystals 0.8 cm wide should provide a resolution of 4-6 mm FWHM over a circular region 30 cm in diameter. Coded lightpipes permit readout using only 56 photomultipliers and 8 coincidence circuits. With properly designed shielding and an energy resolution of 30% FWHM, a positron activity of 200 μCi per axial cm in a 20 cm diam cylinder of tissue should provide approximately 7000 events per sec from a 2 cm thick transaxial section (including a 5% accidental background and a 26% scattered coincident background). This rate is adequate for both static and dynamic imaging.

INTRODUCTION

A clear and valuable goal in nuclear medicine is the rapid, quantitative three-dimensional imaging of isotope distributions within the human body. One realization of this goal is the use of positron emitting pharmaceuticals coupled with a ring of detectors completely surrounding the body (1-4). There are several factors that make this approach timely and attractive: (a) Coincident detection of back-to-back annihilation radiation exploits a much larger solid angle than single gamma imaging, resulting in a great increase in imaging efficiency. (b) The use of a ring of detectors shielded from activity external to the section being imaged provides discrimination against gamma rays scattered in the patient. (c) A large ring of closely packed detectors can provide a sufficiently large number of viewing angles to eliminate the need to rotate the detector system or the patient during exposure. (d) In recent years much progress has been made in the mathematical techniques of computerized transaxial tomography (5-6). This, coupled with the fact that attenuation corrections are easily made for the coincident detection of annihilation radiation gives us the potential for the quantitative determination of the distribution of activity on a μCi per cm^3 basis. (e) In recent years progress has also been made in the production and availability of positron emitting isotopes [e.g., cyclotron-produced 20-min ^{11}C, 10-min ^{13}N, 2-min ^{15}O, 1.8-hr ^{18}F, 4.6-hr ^{81}Rb, 9-hr ^{52}Fe, 9-hr ^{62}Zn; and generator-produced 68-min ^{68}Ga (from 280-day ^{68}Ge), and 1.3-min ^{82}Rb (from 25-day ^{82}Sr)] . A few of the many references to clinical applications of such isotopes may be found in references (7-8). In addition, many other positron emitting pharmaecuticals are being developed for nuclear medicine (9).

BACKGROUND

The application of positron detection in nuclear medicine was suggested in the early 1950's by Wrenn and co-workers (10) and Brownell and Sweet (11). Later, Anger presented a positron imaging system using a scintillation camera in coincidence with a crystal array (12). Use of positron detection devices in clinical medicine was limited by inadequate speed resulting in saturation at relatively low activity levels, such as 300 μCi. This speed limitation has been overcome in part by the MGH camera, which employs two parallel rectangular detector arrays each having 127 NaI(Tl) crystals and 72 photomultipliers (13). Efficient transaxial tomography using this system involves patient or detector rotation, and dynamic flow studies are not possible except indirectly through use of the equilibrium image method (14).

The ring detector system concept was introduced in 1962 by a group at Brookhaven National Laboratory utilizing coincident positron detection for transaxial tomographic imaging (1). The device consisted of 32 NaI(Tl) crystals. Adequate mathematical techniques capable of solving the image reconstruction problem were not employed until recently (2). Phelps, Ter-Pogossian, and co-workers reported on a similar device with a resolution of 11 mm FWHM using 24 NaI(Tl) detectors in a hexagonal pattern (3,4). A 48-detector system, large enough for human use, has been constructed and is now being tested.

In this paper we present the results of a design study on positron ring detectors for transaxial tomography. Our analysis is based on the goal of achieving a combination of good spatial resolution, high sensitivity, rejection of gamma rays that scatter in the tissue or in the detector, variable section thickness, and economic feasibility. This is the first report of a coded light pipe scheme for a ring of detectors.

SPATIAL RESOLUTION

One means of realizing good spatial resolution is by using a large number of small crystals. For example, for an 80-cm diam ring of NaI(Tl) crystals, each 0.8 cm wide and 5 cm deep, the resolution is 4 mm FWHM at the center of the ring and 6.5 mm FWHM at a distance of 15 cm from the center of the ring (fig. 1). The transaxial resolution deteriorates with increasing distance from the ring axis because of the increase in the apparent size of the crystals (fig. 2). (For a detailed analysis, see reference 15). For this detector ring of 280 crystals, it is difficult to optically couple each crystal to a photomultiplier tube (PMT) because of the large number of crystals and the close physical packing.

This problem can be overcome by dividing the detector ring into segments and optically coupling each crystal to several PMT's using a code that uniquely specifies its position within the segment (16). An example of such a code for ten crystals and five PMT's is shown in fig. 3. Each crystal is optically coupled to two PMT's via lightpipes and each lightpipe corresponds to a logic ONE in the truth table. When a crystal scintillates, its digital position code is directly available by interrogating the output of the PMT's.

By representing each crystal with the same number of logic ONE's it is possible to reject events where a significant amount of energy has been deposited in more than one crystal of a segment, since in such cases

more than the prescribed number of PMT's will respond. This can occur when a gamma ray scatters in the crystals or when two gamma rays are detected in the same segment within the coincidence resolving time.

In general, the maximum number of distinct combinations is given by

$$\frac{n!}{m!\ (n-m)!}$$

where n is the number of PMT's serving each segment and m is the number of PMT's to which each crystal is coupled. In the example of fig. 3 the code for a segment containing 10 crystals used n = 5 and m = 2.

The number of PMT's is minimized when $m \approx n/2$. The use of binary and Gray codes will reduce the number of PMT's somewhat further, but will not permit the rejection of multiple detections. The fast digital coding of crystal positions allows each segment to be placed in coincidence with several opposing segments at high rates using a small number of coincidence circuits. Then crystal address codes can be compared to place each crystal in coincidence with a predetermined number of opposing crystals.

In the case of 8 segments of 35 crystals each, the choice of n = 7 and m = 3 allows 56 PMT's to serve 280 crystals via 840 lightpipes and 8 coincidence circuits.

ENERGY AND TIME RESOLUTION

The energy resolution of a scintillation detector depends on the amount of scintillation light produced, the light collection efficiency, and the quantum efficiency of the PMT at the relevent wavelengths. A 5 cm diam X 5 cm NaI(Tl) crystal can achieve an energy resolution of 8% FWHM for 511 keV gamma rays, but any reduction in the light reaching the PMT(such as through the use of narrow crystals or by coupling the crystal to the PMT via a long light pipe) will degrade the resolution.

Grenier et al. report an energy resolution of 23% FWHM at 122 keV and

10% FWHM at 662 keV for a 9 x 9 x 38 mm NaI(Tl) crystal coupled directly to a PMT; and a resolution of 50% FWHM at 122 keV when the same crystal was coupled to the PMT via a 61 cm long lightpipe that transmitted 20% of the light. (17) Their data show that, as expected, the width of the photopeak is inversely proportional to the square root of the number of photons reaching the PMT. As the crystals listed in the example of Table 1 are similar in size and would be coupled to the PMT's via similar lightpipes, we can thus expect that at 511 keV the energy resolution will be approximately 50% FWHM x (122 keV/511 keV)$^{\frac{1}{2}}$ = 24% FWHM. Any non-uniformity among the lightpipes will result in a further degradation of the resolution.

The time resolution in NaI(Tl) depends on the same statistical fluctuations that determine the energy resolution. Braunsfurth et al. report a time jitter distribution with a FWHM of 1.3 nsec for 511 keV gamma ray pairs in NaI(Tl), using a system with a good light collection efficiency (18). We expect that the time jitter distribution of a ring detector system with an energy resolution of 24% FWHM will have a FWHM of 1.3 nsec x (24%/8%) = 3.9 nsec. A 10 nsec coincidence resolving time is assumed in Table 1.

SENSITIVITY

The true coincident event rate C_t of a ring detector is approximated by:

$$C_t = \left[\frac{\rho a S}{2}\right]\left[\frac{S\,(1-P_s)^2}{2c}\right]\left[\varepsilon^2\right] = \frac{\rho a S^2 (1-P_s)^2\,\varepsilon^2}{4c} \qquad (1)$$

where

ρ = activity density in μCi per axial cm

a = 37,000 annihilations per sec per μCi of β^+ (conversion factor)

S = exposed dimension of detector ring along ring axis (determined by width of shielding slit - see fig. 4)

c = radius of detector ring

P_s = probability that a 511-keV gamma ray will scatter on passing through half the tissue

ε = detection efficiency for 511-keV gamma rays.

The first bracket is the contributing activity; the second bracket is the probability that both gamma rays reach the detector ring without having scattered; and the third bracket is the probability that both gamma rays are detected and pass the pulse height threshold.

We assume that the source distribution lies within a distance R from the ring axis given by:

$$R = c \sin (f\pi/2) \qquad (2)$$

where each detector (of a total of N) is in coincidence with the fN opposing detectors. For a circular ring the geometrical sensitivity is nearly uniform within the radius R. We also assume that the detectors are densely packed around the ring and that the shielding blocks only gamma rays external to the section being imaged.

In Table 1 we have calculated the sensitivity C_t/ρ and many other parameters for a particular positron ring detector system and a tissue thickness of 20 cm. In this example the event rate is 5000 to 7000 events per sec for ρ = 200 μCi per axial cm. Thus if the section is to be resolved into a grid of 40 x 40 pictels, 300 to 400 events can be collected per pictel over a 100-sec time period. Let us also consider the case of gated imaging of the myocardium using generator produced 75-sec ^{82}Rb. We assume that (a) the heart is 10 cm in the cephlad-caudad dimension, and the myocardial volume is 150 cm^3; (b) the cardiac rate is 72 min^{-1}; (c) the scattering medium is equivalent to a 20 cm diam cylinder of tissue; (d) 20 mCi of ^{82}Rb is injected i.v. and 3.5% of this is extracted by the

myocardium; (e) twelve separate images are taken, each corresponding to a 0.1 sec interval of the 1.2 sec cardiac cycle; (f) Data are taken for a period of 200 sec after an initial 100 sec wait for the blood pool clearance of ^{82}Rb; (g) As in Table 1, Case II, the imaging sensitivity is 23 events sec^{-1} $\left[\mu Ci \text{ per axial cm}\right]^{-1}$. The resulting initial activity density is 0.7 μCi per 4 x 4 x 10 mm image element and for each of the twelve images typically 90 events will be collected per image element.

SHIELDING AND BACKGROUNDS

Shielding is essential for blocking gamma rays emitted by activity external to the section being imaged. Furthermore, varying the width of the shielding slit allows the section thickness to be varied. True unscattered coincident events can arise only from a positron activity $\frac{\rho S}{2}$ within the section, but scattered coincident events and single counts (both of which contribute to the background) can arise from an activity that is effectively $\frac{\rho c S}{T}$, where T is the depth of the shielding slit (fig. 4).

There are two methods available for rejecting scattered gamma rays. The coincidence requirement (i.e., that each of the N detectors be in coincidence with the fN opposing detectors) establishes an approximate upper limit $\Theta_f = f\pi$ on the scattering angle. This approximation is realistic, as the size of the scattering medium is usually small compared to the diameter of the detector ring. The second method is the use of a pulse height threshold that rejects scattered gamma rays with an energy below E_p. In single Compton scattering this corresponds to a maximum scattering angle Θ_p (19 eqn. 8 e-5):

$$\cos(\Theta_p) = 2 - \frac{511 \text{ keV}}{E_p} \qquad (3)$$

For scattered coincident events the effective maximum scattering angle Θ_m is the smaller of Θ_f and Θ_p. (For single counts the maximum

scattering angle is always θ_p.) The effective minimum scattered gamma ray energy E_m corresponding to θ_m is given by:

$$E_m = \frac{511 \text{ keV}}{2 - \cos(\theta_m)} \tag{4}$$

The rate of scattered coincident events where only one member of the annihilation pair scatters is approximated by:

$$C_1 = \left[\frac{\rho a S c}{T}\right]\left[\frac{S(1-P_s)}{c}\right]\left[\frac{P_s g_1 S}{c}\right]\left[\varepsilon\varepsilon_m\right] = \frac{\rho a S^3 g_1 \varepsilon\varepsilon_m P_s(1-P_s)}{Tc} \tag{5}$$

where the quantity ε_m is the average detection efficiency for gamma rays between energy E_m and 511 keV, and g, is a solid angle factor. The first bracket is the contributing activity; the second bracket is the probability that either gamma ray reaches a detector without scattering; the third bracket is the probability that the other gamma ray scatters and reaches one of the opposing (coincident) detectors; and the fourth bracket is the probability that both gamma rays are detected and pass the pulse height threshold. This expression assumes that the activity is near the center of the scattering medium, that the scattering takes place close to the axis of the ring and that single scattering predominates.

The dimensionless quantity g_1 describes the fraction of Compton scattering angles that fall within the angular strip S/c wide and $2\theta_m$ long:

$$g_1 = \frac{\int_{-\theta_m}^{\theta_m} \frac{d\sigma}{d\Omega}\, d\theta}{\int_0^{\pi} 2\pi \frac{d\sigma}{d\Omega} \sin\theta\, d\theta} \tag{6}$$

where $\frac{d\sigma}{d\Omega}$ is the differential cross section for Compton scattering of 511 keV gamma rays on free electrons, given by the Klein-Nishina formula: (ref. 19 eqn. 8e-13).

$$\frac{d\sigma}{d\Omega} = 11.91 \times 10^{-26} \text{ cm}^2/\text{str/electron} \frac{(1-\cos\theta + \cos^2\theta - \frac{1}{3}\cos^3\theta)}{(2-\cos\theta)^3} \quad (7)$$

where θ is the γ-ray scattering angle. See Table 2 for values of g_1 as a function of θ_m.

The rate of scattered coincident events C_2 where both members of the annihilation pair have scattered is approximated by:

$$C_2 = \left[\frac{\rho a S c}{T}\right]\left[\frac{SP_s}{2e}\right]\left[\frac{P_s g_2 S}{c}\right]\left[\epsilon_m^2\right] = \frac{\rho a\, S^3 g_2\, \epsilon_m^2\, P_s^2}{2Tc} \quad . \quad (8)$$

The first bracket is the contributing activity, the second bracket is the probability that one gamma ray scatters and reaches the detectors; the third bracket is the probability that the other member of the pair also scatters and reaches one of the opposing (coincident) detectors; and the fourth bracket is the probability that both gamma rays are detected and pass the pulse height threshold. Assuming that single scattering predominates for each gamma ray, g_2 is given by

$$g_2 = \frac{\int_{-\theta_m}^{\theta_m} \frac{d\sigma^*}{d\Omega}\, d\theta}{\int_0^{\pi} 2\pi \frac{d\sigma^*}{d\Omega} \sin\theta\, d\theta} \quad (9)$$

where $\frac{d\sigma^*}{d\Omega}$ is the autocorrelation of $\frac{d\sigma}{d\Omega}$. See Table II for approximate values of g_2 as a function of θ_m. The total background rate C_b from

scattered coincident events is given by:

$$C_b = C_1 + C_2 = \frac{\rho a S^3}{2T_c}\left[2g_1\ \varepsilon\varepsilon_m P_s(1-P_s) + g_2\ \varepsilon_m^2 P_s^2\right]. \qquad (10)$$

Note that the backgrounds C_1 and C_2 are not associated with time resolution but with scatter geometry and energy resolution. As expected, the ratio of scattered coincident events C_b to true unscattered coincident events C_t is lowest for "good scatter geometry" (i.e., small S/T).

The single counting rate C_s is given by:

$$C_s = \left[\frac{2\rho a S c}{T}\right]\left[\frac{S}{2c}\right]\left[\varepsilon(1-P_s) + \varepsilon_p P_p\right] = \frac{\rho a S^2}{T}\left[\varepsilon(1-P_s) + \varepsilon_p P_p\right] \qquad (11)$$

where P_p is the probability that a gamma ray will scatter in tissue and retain an energy greater than E_p (i.e., the pulse height threshold) and ε_p is the average detection efficiency for such gamma rays. The first bracket is the contributing activity; the second bracket is the solid angle factor of the detector ring; and the third bracket is the sum of the probability for not scattering and being detected and the probability for scattering and being detected. For the single Compton scattering of 511-keV gamma rays,

$$P_p \approx P_s\left[\frac{5/2 + 3\ \ell n\alpha\ + 1/\alpha - 3\alpha - \alpha^2/2}{40/9 - 3\ \ell n3}\right] \qquad (12)$$

where $\alpha = E_p/511$ keV and $1/3 \leq \alpha \leq 1$. The quantity in brackets is the probability that the scattered photon will have an energy greater than E_p, derived by integrating eqn. 8e-21 of ref. 19.

The accidental coincidence rate C_a is given by:

$$C_a = fC_s^2 t \tag{13}$$

where t is the time resolution. It is of importance to calculate the maximum rate $\hat{C}_t$ for a certain fraction $\eta = C_a/C_t$ of accidental coincidences:

$$\hat{C}_t = \frac{\eta T^2 \varepsilon^4 (1-P_s)^4}{16\, ftc^2 \left[\varepsilon(1-P_s) + \varepsilon_p P_p\right]^2} \tag{14}$$

As expected, the maximum event rate is enhanced by good time resolution, good shielding, and good detection efficiency. It is important to reduce f to the point where all (or almost all) of the activity lies within the radius R (eqs. 2). Reducing f below this value will reduce the signal C_t approximately as f^2 (without effecting the single counting rate C_s) and actually cause $\hat{C}_t$ to decrease.

For the example of Case II of Table 1 and for a 10% accidental coincidence rate ($\eta = 0.10$), we have

$$\hat{C}_t = 6990 \text{ events per sec}$$

and

$$\rho = 305 \ \mu\text{Ci per axial cm.}$$

The profound effect that the scattering medium has on the maximum event rate can be seen by noting what these values would be in the absence of the scattering medium (i.e., $P_s = P_p = 0$):

$$\hat{C}_t = 130{,}000 \text{ events per sec}$$

and

$$\rho = 780 \ \mu\text{Ci per axial cm.}$$

One should note that: (a) increasing T (whenever possible) by extending the collimator closer to the patient reduces all backgrounds without reducing the sensitivity; (b) Increasing the section thickness S increases the sensitivity as S^2, but the scattered coincident background increases as S^3; (c) The maximum event rate $\hat{C}_t$ (as limited by accidentals) is not a function of S.

DEADTIME

Deadtime arises from the limited speed of both the scintillation process and the electronic circuits. After the interaction of a gamma ray in NaI(Tl), 800 nsec is required to collect 90% of the available scintillation light (91% of the light is emitted with an exponential time constant of 218 nsec and 9% is emitted with an exponential time constant of 1340 nsec) (20). To preserve pulse height information to within 10% at high counting rates it is therefore necessary to reject all counts that occur within approximately 800 nsec of another count. This requirement results in a paralyzing deadtime of 800 nsec for each coded segment of the ring. The circuits that perform the pulse height selection may also introduce a paralyzing deadtime, but by proper design (21) it is possible to limit the overall paralyzing deadtime t_p to 1 μsec. The circuits that handle the time coincidence and position information introduce a non-paralyzing deadtime t_n of $\leq$ 200 nsec, but this does not result in an appreciable loss of counts, provided the circuits are properly designed and $t_n \leq t_p$.

In Cases II and III of Table 1, where a pulse height selection is imposed, the fraction of time that each 35 crystal segment is available is e^{-Gtp}, and the fraction of counts f_c lost per segment is given by:

$$f_c = 1 - e^{-Gt_p}. \qquad (15)$$

G is the gross counting rate for each segment (1.3×10^5), t_p = 1 μsec, and the fraction of counts lost (f_c) is 12%. As a coincident event requires that two segments be available for counting (probability = e^{-2Gt_p}), the fraction of coincident events f_e lost is given by

$$f_e = 1\text{-}e^{-2Gt_p} \qquad (16)$$

and equal to 23% for this example.

In Case I of Table 1 no pulse height selection is imposed and we assume that the paralyzing deadtime can be reduced to 200 nsec. In this case the fraction of counts lost (f_c) is 2.5% and the fraction of events lost (f_e) is only 5%, but the backgrounds are larger (see Table 1)

RECONSTRUCTION METHODS

For the ring detector system of densely packed crystals presented in this analysis, each of the 280 crystals is in coincidence with 62 opposing crystals, providing 8680 crystal pair combinations. Four possible methods of reconstruction are envisioned (for reviews of reconstruction techniques, see refs. 5 and 6). The first method is to generate a back-projection image from the distribution of lines connecting coincident detector pairs. Reconstruction is accomplished using two-dimensional Fourier transform techniques. The second method is to store the lines connecting coincident detector pairs into bins corresponding to intervals of direction and position. The data are then reconstructed using the algorithm of back projection of filtered projections. The third method is to multiply either the back-projection image or the binned data by the generalized pseudo-inverse matrix, which has been derived for the particular geometry of the system.

The fourth method is the use of the closed-form expressions of Marr that permit the activity distribution to be estimated directly from a list of the coincident detector pairs (22).

ATTENUATION CORRECTIONS

Although the corrections for attenuation are much smaller for coincident annihilation imaging than for single gamma imaging, some correction is needed to obtain good transaxial reconstructions. One possibility is the use of a continuous source of positron emitter around the outside of the patient, as suggested by Phelps et al. (3). Since the attenuation depends only on the line of flight of the two gamma rays and not on the position of the point of annihilation, the attenuation correction for each pair of coincident detectors is the ratio of the transmitted flux before and after the patient is positioned in the system.

A second possibility is the use of a fan beam source of 7.8-yr ^{133}Ba (principal gamma energy 356 keV) that travels 180 degrees around the patient while the opposing 62 crystals collect transmission data. As the attenuation cross section is greater at 356 keV than at 511 keV by a factor of 1.16 for water, muscle and bone (23), the attenuation correction for 511-keV pairs is determined as the 0.86 power of the ratio of the transmitted flux of 356 keV gamma rays before and after the patient is positioned in the system. It is necessary to know the attenuation to an accuracy of only 10% rather than the 1% accuracy of the EMI scanner, and approximately 100 times fewer counts are needed. Thus the dose is reduced from 1-3 rad to 50-150 mrad. This second method permits greater ease of source collimation to reduce patient exposure, greater data rates, and the use of an isotope of long half life.

In summary, we have presented an analysis of the potentials and limitations of a new scheme for the high resolution imaging of positron emitting pharmaceuticals in nuclear medicine. With an activity density of 200 μCi/cm (typically 5-20 mCi in the patient) and an energy resolution of 30% FWHM, the device should operate at 7000 events per sec, including a 5% accidental background and a 26% scattered coincident backbround. Relaxation of the pulse height threshold to 100 keV eliminates the need for some circuits and improves deadtime, but increases the background event rates. This system has the speed capability for dynamic imaging of brain blood flow (e.g. using ^{11}C, ^{15}O, ^{82}Rb, ^{68}Ga on appropriate compounds) and myocardial uptake of nuclides [e.g., ^{82}Rb (24) or ^{13}N-labeled L-asparagine (25)] as well as high spatial resolution imaging of head, thorax, abdomen, and pelvis.

ACKNOWLEDGMENTS

This work was supported in part by NIH grant 1 R01 GM-20115-02 RAD and in part by the U.S. Energy Research and Development Administration.

TABLE 1. PROPERTIES OF A RING DETECTOR SYSTEM[a] FOR THREE ASSUMED ENERGY RESOLUTIONS

Quantity	Symbol	Units	Case I	Case II	Case III
Energy resolution (FWHM) at 511 keV	Γ	%	none	30	15
Energy threshold	E_p	keV	100	410[b,c]	460[b,c]
Approximate maximum scattering angle corresponding to E_p (eqn.3)	θ_p	degrees	180	41	27
Effective maximum scattering angle	θ_m	degrees	40	40	27
Minimum scattered gamma energy corresponding to θ_m (eqn.4)	E_m	keV	415	415	460
Average detection efficiency for gamma ray energies from E_m to 511 keV	ε_m	%	65	48	45
Detection efficiency for 511 keV gammas	ε	%	53	43	43
Probability that a 511 keV gamma ray will scatter and retain an energy above E_p (eqn. 12)	P_p	%	63	20	10
Average detection efficiency for gamma ray energies from E_p to 511 keV	ε_p	%	80	48	45
Geometry factor - one gamma scatters (eqn. 6)	g_1	--	0.31	0.31	0.23
Geometry factor - both gammas scatter (eqn. 9)	g_2	--	0.19	0.19	0.13
Rate for true unscattered coincident events (eqn. 1)	C_t	events per sec	7100	4700	4700
Sensitivity	C_t/ρ	events per sec per $[\mu Ci/cm]$	36	23	23

TABLE 1 (cont.)

Quantity	Symbol	Units	Case I	Case II	Case III
Coincidence rate for one gamma scatter (eqn.5)	C_1	events per sec	1840	1100	770
Coincidence rate for two gamma scatter (eqn.8)	C_2	events per sec	1180	640	390
Singles rate for entire ring (eqn.11)	C_s	10^5 events per sec	10.4	3.8	3.0
Accidental coincidence rate for entire ring (eqn.13)	C_a	events per sec	2400	320	200
Total event rate ($C_t + C_1 + C_2 + C_a$)		events per sec	12520	6760	6060
Background fraction $\frac{C_1+C_2+C_a}{C_t+C_1+C_2+C_a}$		%	43	30	22
Paralyzing deadtime	t_p	nsec	200	800	800
Fraction of events lost due to deadtime[c] (eqn.16)	f_e	%	5	23	23

[a]Physical specifications of assumed ring detector system are as follows:

c = detector ring radius = 40 cm

S = shielding slit width = 2 cm

T = shielding slit depth = 20 cm

P_s = probability of scattering on emerging from the center of a 20 cm diam cylinder of tissue = 63%

f = 0.22 (for 280 crystals, each would be in coincidence with the opposing 62 crystals)

θ_f = 40^o maximum scattering angle imposed by coincidence requirement (approximate)

ρ = activity density = 200 μCi per axial cm

t = time resolution = 10 nsec

dimension of crystals along gamma line of flight = 5 cm

dimension of crystals along ring axis = 3 cm

dimension of crystals transverse to ring axis = 0.8 cm

R = radius of uniform geometrical sensitivity = 14 cm

G = gross singles rate per segment = 1.3×10^5 counts per sec

[b]Corresponds to a 7% photopeak loss, assuming that the photopeak has a Gaussian distribution.

[c]This event loss has not been included elsewhere in this table.

TABLE 2. THE GEOMETRICAL FACTORS g_1 AND g_2 AS A FUNCTION OF THE MAXIMUM EFFECTIVE SCATTERING ANGLE θ_m

θ_m	g_1	g_2
0^o	0	0
10^o	0.10	0.05
20^o	0.18	0.10
30^o	0.26	0.15
40^o	0.31	0.19
50^o	0.36	0.23
60^o	0.40	0.26

REFERENCES

1. Rankowitz S, Robertson JS, Higinbotham WA, et al: Positron scanner for locating brain tumors. IRE International Convention Record, 10(9):49-56, 1962

2. Robertson JS, Marr RB, Rosenblum M, et al: 32 crystal positron transverse section detector. Tomographic Imaging in Nuclear Medicine, New York, Society of Nuclear Medicine, 1973, pp. 142-153.

3. Phelps ME, Hoffman EJ, Mullani, NA, et al: Application of annihilation coincidence detection to transaxial reconstruction tomography. J Nucl Med, 16: 210-224, 1975

4. Ter-Pogossian MM, Phelps ME, Hoffman EJ, et al: A positron-emission transaxial tomograph for nuclear imaging (PETT). Radiology, 114:89-98, 1975

5. Gordon R, Herman GT: Three dimensional reconstruction from projections: a review of algorithms, Int. Rev. Cytol. 38: 111-151, (1974)

6. Budinger TF, Gullberg GT: Three-dimensional reconstruction in nuclear medicine emission imaging. IEEE Trans 21(3): 2-20, 1974

7. Glass HI: New applications of radiopharmaceuticals labeled with cyclotron-produced radionuclides. Symposium on Medical Radioisotope Scintigraphy, vol 2, Monte-Carlo 1972, pp 299-324

8. Silvester DJ, Clark JC, Palmer AJ: The future of accelerator-produced radiopharmaceuticals. Proc First World Congress of Nuclear Medicine, Tokyo, Sept. 30-Oct. 4, 1974, pp. 181-190

9. Proceedings of the International Symposium on Radiopharmaceuticals, Atlanta, Georgia, Feb. 1974. To be published by the Soc Nucl Med

10. Wrenn FR, Good ML, Handler P: The use of positron-emitting radioisotopes for the localization of brain tumors. Science 113:525-527, 1951

11. Brownell GL, Sweet WH: Localization of brain tumors. Nucleonics 11(11): 40-45, 1953

12. Anger HO: Survey of radioisotope cameras. Inst. Soc. Am. Trans. 5:311-334, 1966

13. Burnham CA, Brownell GL: A multi-crystal positron camera, IEEE Trans 19(3):201-205, 1972

14. Jones T, Brownell GL, Ter-Pogossian MM: "Equilibrium" images of short-lived radiopharmaceuticals for dynamic observations. J Nucl Med 15:505 (abstract) (1974)

15. Derenzo SD, Zaklad H, Budinger TF: Positron Emission Camera for Transverse Section Tomography. Lawrence Berkeley Laboratory Report No. LBL-2848, 1975 (unpublished)

16. Alvarez LW: A new γ-ray imaging camera, Group A Physics Note No. 784, May 1974, available from Group A, Lawrence Berkeley Laboratory, Berkeley CA 94720, (unpublished).

17. Grenier RP, Bender MA, Jones RH: A computerized multi-crystal scintillation gamma camera. In Instrumentation in Nuclear Medicine, Vol 2 Hine GJ, Sorenson JA (edit), Academic Press, New York, 1974

18. Braunsfurth J, Körner HJ, Zeitauflösungseigenschaften von NaJszintillatoren, Nucl Instr Meth 34:202-212, 1965

19. Gray DE(edit): American Institute of Physics Handbook, 3rd edition, McGraw-Hill, New York, 1972

20. Tidd JL, Dabbs JR, Levine N: Scintillator handbook with emphasis on cesium iodide, NASA technical memorandum No. NASA TM-X-64741, April 1973, available from the National Technical Information Service, Springfield, VA 22151, (unpublished).

21. Blatt SL, Mahieux J, Kohler D: Elimination of pulse pileup distortion in nuclear radiation spectra. Nucl Inst. Meth 60: 221-230, 1968

22. Marr RB: On the reconstruction of a function on a circular domain from a sampling of its line integrals. J Math Anal Appl 45:357-374, 1974

23. Hubbell JH: Photon Cross Sections, Attenuation Coefficients, and Energy Absorption Coefficients from 10 keV to 100 GeV. U. S. Nat. Bur. Stand. Report NSRDS-NBS 29, 1969

24. Budinger TF, Yano Y, and Hoop B: A comparison of $^{82}Rb^{+}$ and $^{13}NH_3$ for myocardial positron scintigraphy, J. Nucl. Med. 16, May 1975.

25. Gelbard AS, Clarke LP, Laughlin JS: Enzymatic synthesis and use of ^{13}N-labeled L-asparagine for myocardial imaging, J Nucl Med 15:1223-1225, 1974

FIGURE CAPTIONS

FIG. 1. FWHM of the transaxial point spread function (averaged over all gamma ray directions) vs the distance to the center of the detector circle. Detector ring is assumed to be 80 cm in diameter and composed of 280 NaI(Tl) crystals each 8 mm wide.

FIG. 2. Detector ring and source (P) showing that for off-axis points the transaxial resolution depends on the gamma ray direction.

FIG. 3. Example showing the coding scheme for 5 photomultipliers and the first 6 of 10 crystals. Lines designate lightpipes having half the cross sectional area of the crystals. The complete code is shown in the truth table where a "ONE" represents a lightpipe connection between a crystal and a PMT. Expansion to 35 crystals requires 3 lightpipes per crystal and 2 additional photomultipliers.

FIG. 4. Illustration showing how Compton scattering can contribute a background to the coincident event rate. Although the two gamma rays are in time coincidence, they are not collinear and do not provide useful spatial information. Unscattered coincident events can only arise from the region between the dashed lines.

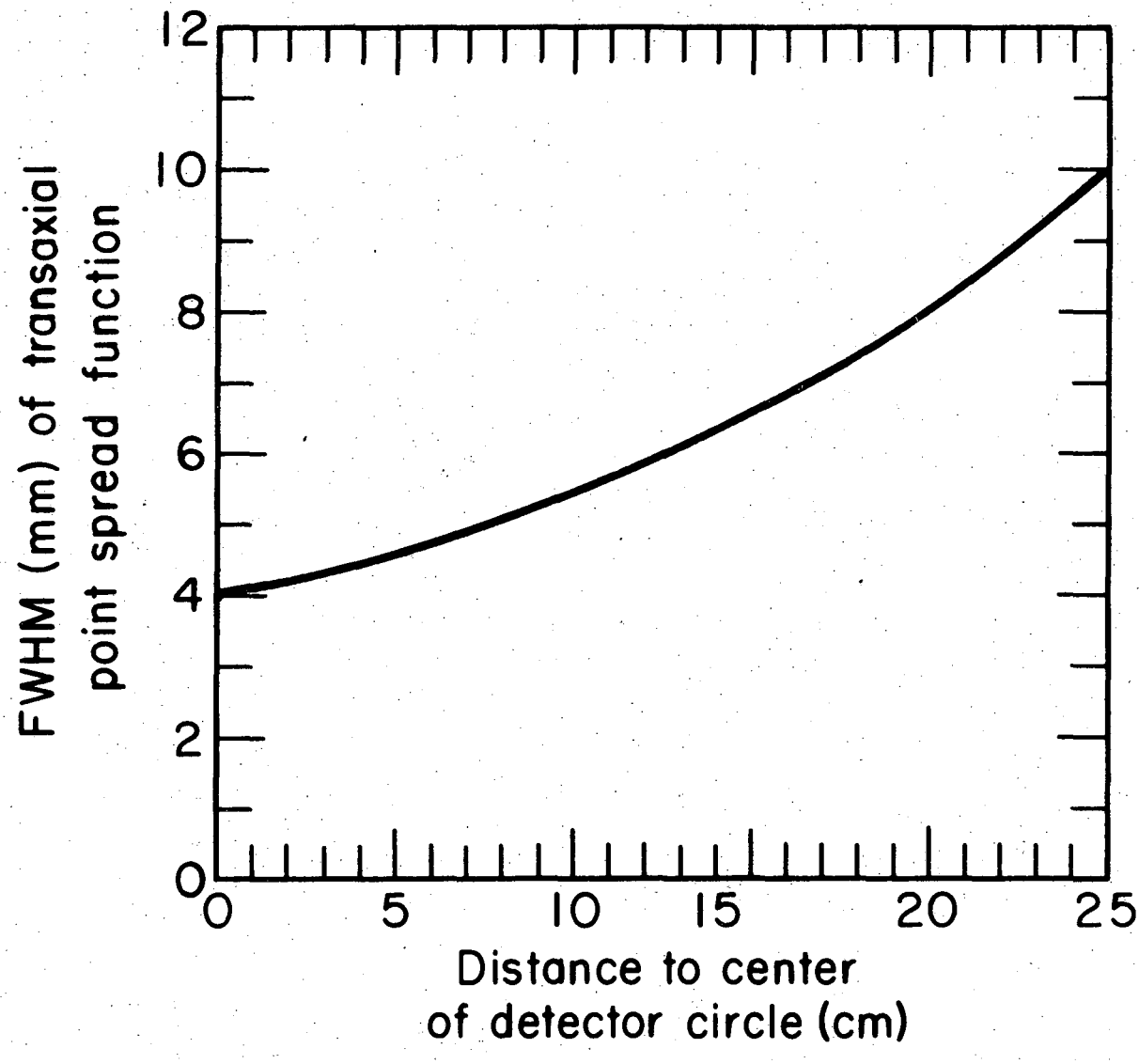

XBL 749-4219

Fig 1

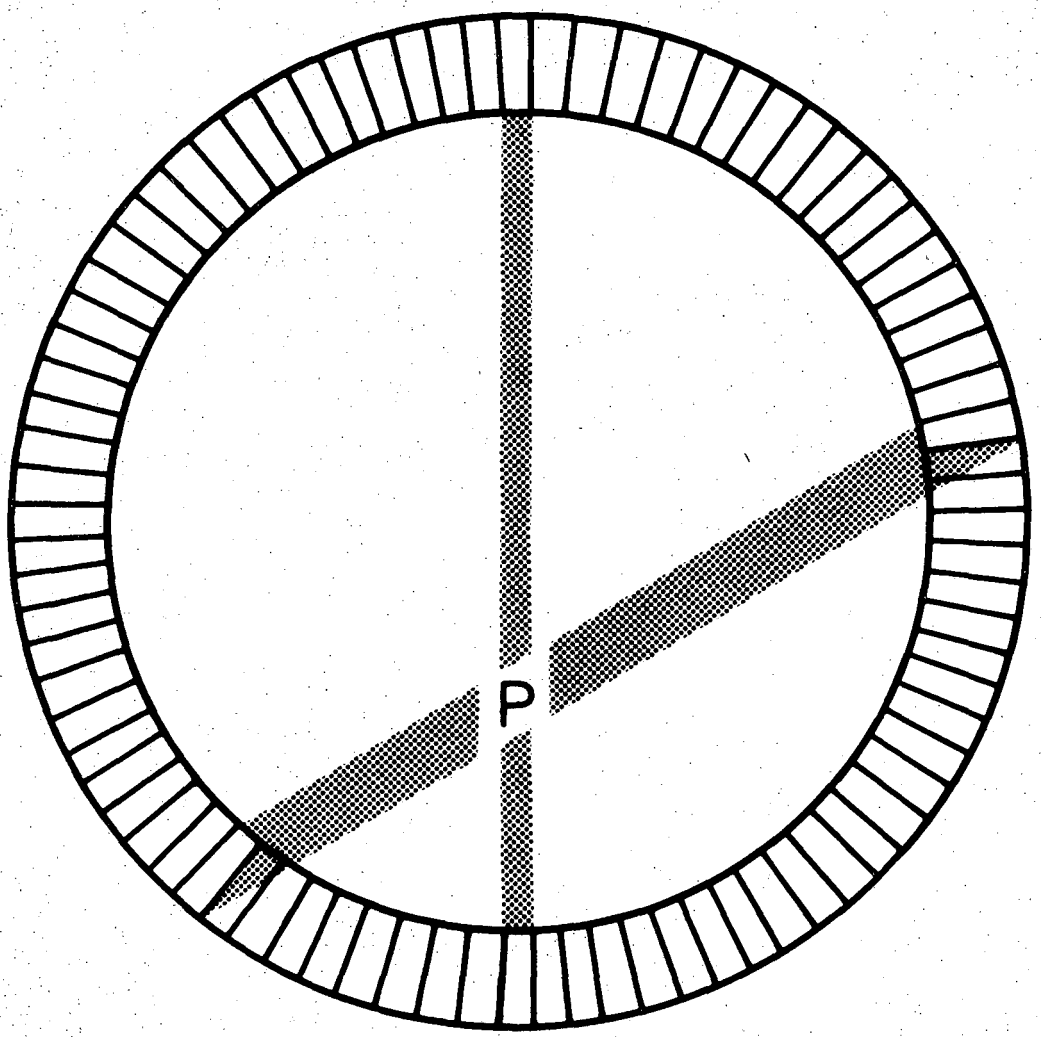

XBL753-2537

Fig 2

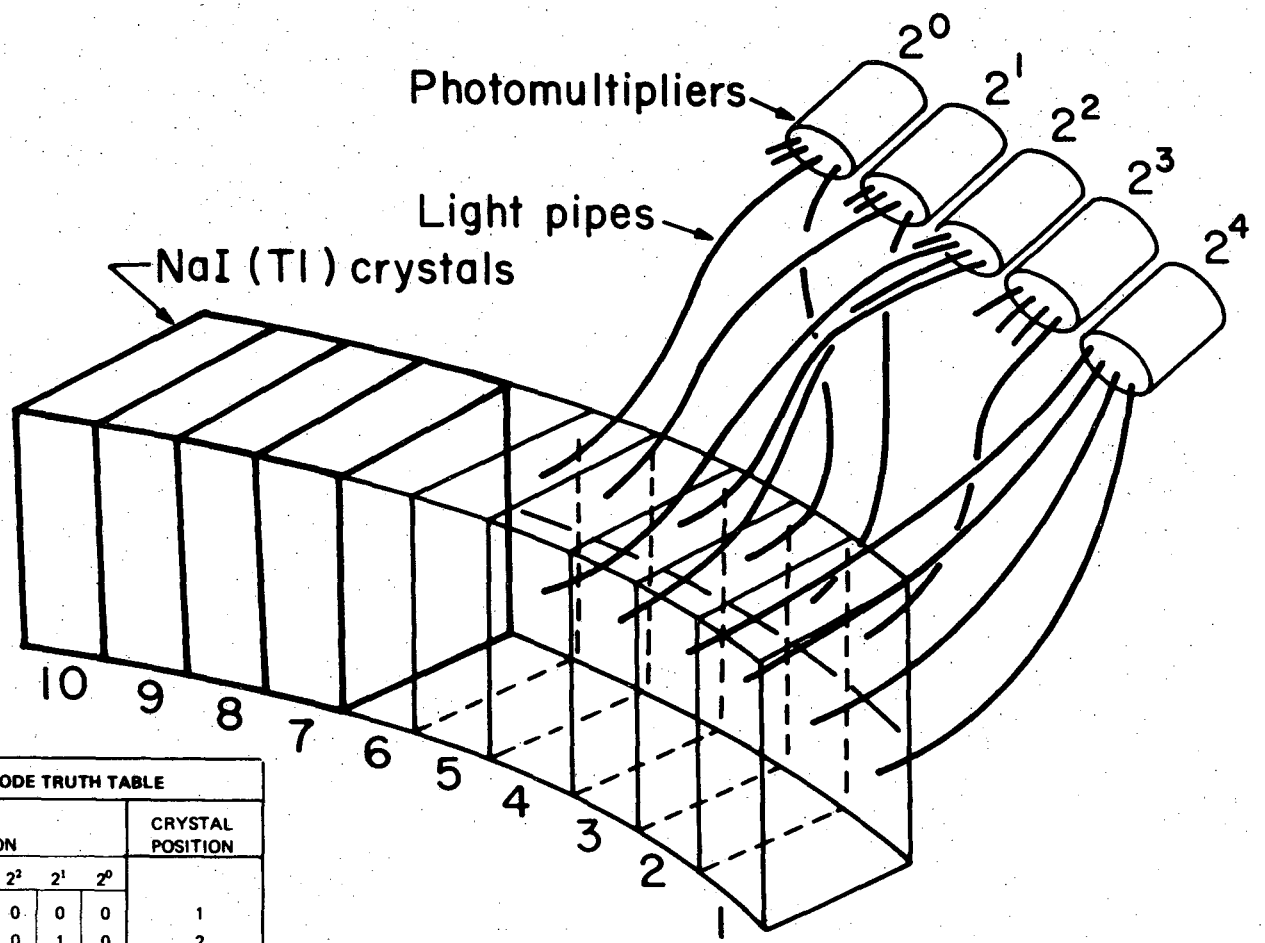

CODE TRUTH TABLE					
PMT CONNECTION					CRYSTAL POSITION
2^4	2^3	2^2	2^1	2^0	
1	1	0	0	0	1
1	0	0	1	0	2
1	0	0	0	1	3
1	0	1	0	0	4
0	0	1	1	0	5
0	0	1	0	1	6
0	0	0	1	1	7
0	1	0	1	0	8
0	1	0	0	1	9
0	1	1	0	0	10

Fig 3

XBL753-2536

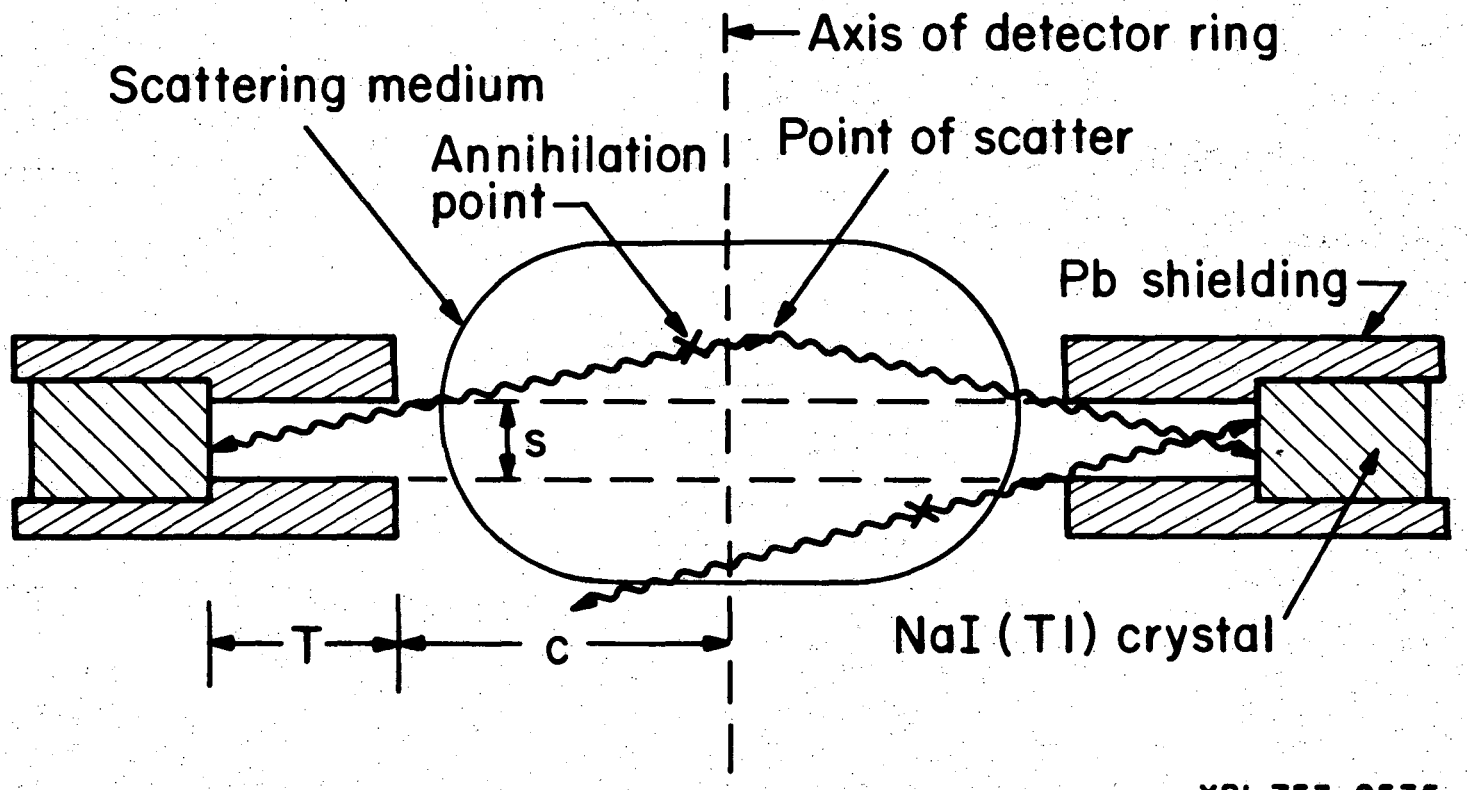
Axis of detector ring
Scattering medium
Annihilation point
Point of scatter
Pb shielding
s
T
c
NaI (Tl) crystal
XBL 753-2535

Fig 4

TECHNICAL INFORMATION DIVISION
LAWRENCE BERKELEY LABORATORY
UNIVERSITY OF CALIFORNIA
BERKELEY, CALIFORNIA 94720